Elaboration, microstructure and reactivity of Cr3C2 powders of different morphology

Sophie Loubière, Christophe Laurent, Jean-Pierre Bonino, Abel Rousset

ELABORATION, MICROSTRUCTURE AND REACTIVITY OF Cr_3C_2 POWDERS OF DIFFERENT MORPHOLOGY

S. Loubière, Ch. Laurent, J. P. Bonino, and A. Rousset
Laboratoire de Chimie des Matériaux Inorganiques, URA CNRS 11311,

ABSTRACT

Cr_3C_2 powders have been prepared by heat-treatment of metastable chromium oxides of controlled morphology in H_2-CH_4 atmosphere. Starting with these highly reactive oxides allows formation of Cr_3C_2 at 700°C. The reaction is pseudomorphic and different grain shapes (needles, rods, spheres and polyhedra) have been obtained. The size distribution is narrow and the grain size is generally of the order of a few tens of micrometers, but the "spheres" are in fact made up of aggregates of small platelets about 1.5 μm wide and 0.7 μm thick. The oxidation in air of the carbides was studied by thermal analyses (TGA, DTG and DSC) and was found to proceed in four steps in the 250-700°C range. The differences observed between the carbides are related to their morphology and texture.

MATERIALS INDEX: Chromium carbide, chromium oxide

INTRODUCTION

The stable chromium carbides (Cr_3C_2, Cr_7C_3 and $Cr_{23}C_6$) have many applications owing to properties such as high hardness, high melting point, resistance to chemical attack, high Young modulus and wear resistance (1). Recently, dispersions of Cr_3C_2 particles in an alumina (2) or a mullite (3) matrix have been prepared using the internal reactions taking place during milling of SiC, Al_2O_3 and Cr_2O_3; these composites exhibit higher mechanical properties than the matrix alone. Several methods have been used for the elaboration of Cr_3C_2 films or powders, including physical vapor deposition (4-10), chemical vapor deposition (11), mechanical alloying (12), combustion synthesis (13) and action of C (14-16), CO (17, 18) or

H_2-CH_4 mixture (19-22) on chromium oxide or on an organometallic salt. Regarding this latter method, it has been shown (20, 21) that it is possible to prepare Cr_3C_2 at temperatures as low as 800°C by using a chromium salt such as a hydroxide, oxalate or formate as the starting compound. Indeed, the salt is decomposed upon the increase in temperature, thus giving rise to a highly reactive chromium oxide which is then carburized at a higher temperature. However, fairly long heat-treatment durations (ten hours or more) are needed and only small quantities can be prepared. Starting with Cr_2O_3 allows us to work on larger quantities, but requires a higher carburization temperature (1100°C). Furthermore, the yield of the reaction is poor (approximately 75%), even when working with a fluidized bed set-up (22).

Lerch and Rousset (23) have recently shown that the decomposition in air of chromium oxalates at the appropriate temperature could lead to metastable chromium oxides of general formula CrO_x (x equal to approximately 1.9). Since the specific surface area of these oxides is in the 200-350 m^2/g range, it was anticipated that they could be starting materials for the synthesis of chromium carbide powders in acceptable amounts while combining the advantages of moderate preparation temperature and high yield. Moreover, the preparation route described by Lerch and Rousset (23) allows us to control the morphology of the oxalate precursors as well as that of the oxides. Little attention has been paid in earlier works to the morphology of the Cr_3C_2 grains, but Paris and Clar (20) mentioned that their Cr_3C_2 powder had a fine-grained microstructure and a higher reactivity to air than a commercial carbide. A controlled morphology would be essential if the powders were to be used for preparing carbide coatings by electrodeposition. In the present paper, we describe the synthesis of Cr_3C_2 powders of different morphology and investigate their air oxidation.

EXPERIMENTAL

The ammonium trioxalatochromate(III) $(NH_4)_3[Cr(C_2O_4)_3]$ were prepared by mixing the appropriate amounts of ammonium oxalate $(NH_4)_2(C_2O_4)$, 2 H_2O (Prolabo 21289.293) and chromium (III) nitrate $Cr(NO_3)_3$, 9 H_2O (Merck 2481.0250) in an aqueous solution (designated AS hereafter) heated at 60°C. The obtained clear solution was cooled to room temperature and rapidly added to an equivolumic mixture (designated OS hereafter) of two organic solutions, in which precipitation occurred immediately. In order to obtain oxalate precursors with different morphology (23), we used two OS, acetone (Carlo Erba 400971)-methanol (Carlo Erba 414814) and ethanol (technical grade)-ethyleneglycol (Prolabo 24041.446) and varied the relative amounts of AS and OS (V_{AS} / V_{OS} ratio). After filtering and ethanol washing, the powders were oven dried at 90°C for 48 hours. The preparative conditions and the corresponding morphologies (needles, rods, spheres and polyhedra) are summarized in Table 1.

The oxalates were decomposed in air at 330°C and the so-obtained CrO_x (x equal to approximately 1.9) (23) were heat-treated in H_2-CH_4 atmosphere. The gas flow was dried on P_2O_5 and its composition was monitored using massflow controllers. The CH_4 proportion in the gas mixture was fixed to 10% in order to prevent its dissociation and the formation of graphite (20, 24). The carburization was carried out at 700°C for two hours.

Phase identification was performed by X-ray diffraction (XRD) patterns analysis using Co Kα radiation (λ = 0.17902 nm). Chemical analysis was done by atomic absorption at CNRS (Solaize, France). The specific surface areas were measured by the BET method using nitrogen adsorption. The powders were observed by scanning electron microscopy (SEM) and transmission electron microscopy (TEM). The oxidation behaviour of the carbides was studied

TABLE 1

Preparative Conditions and Morphology of the Different Oxalates

Precipitation medium (vol. %)	Acetone-methanol (50/50)		Ethanol-ethyleneglycol (50/50)	
V_{AS}/V_{OS} Morphology	0.066 needles	0.1 rods	0.050 spheres	0.1 polyhedra

by thermogravimetric analysis (TGA), differential thermogravimetric analysis (DTG) and differential scanning calorimetry (DSC) carried out in flowing air. The heating rate for TGA and DSC measurements was fixed at 2° and 1°C/min, respectively.

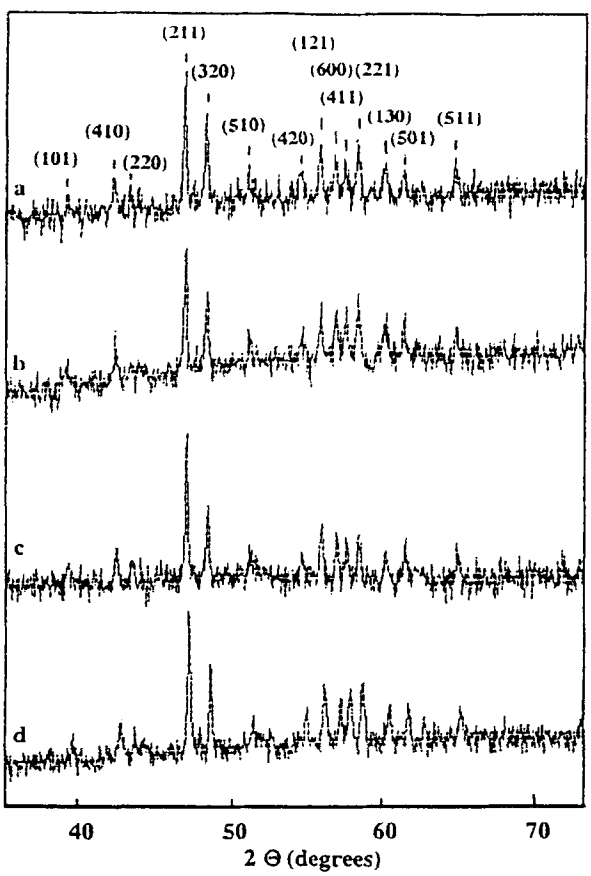

FIG. 1

XRD patters of the Cr_3C_2carbides obtained by carburization at 700°C (2 h, 10% CH_4) of the different oxides: (a) needles; (b) rods; (c) spheres; (d) polyhedra.

RESULTS AND DISCUSSION

Microstructure. XRD patterns analysis of the different carburization products revealed the presence of Cr_3C_2 only (Fig. 1). The diffraction peaks are very narrow, showing a high crystallization level of thecarbides. It is noteworthy that no remaining Cr_2O_3 is detected despite the low preparation temperature (700°C) used, which is slightly below the one (750°C) indicated by thermodynamic calculations (20) for the beginning of the reaction

$$3Cr_2O_3 + 13CH_4 \rightarrow 2Cr_3C_2 + 9CO + 26H_2$$

in the same conditions of pression. Atomic absorption analysis showed that the Cr_3C_2 powders contain approximately 1.5% free carbon, less than 0.8% oxygen, less than 0.2% nitrogen and less than 0.09% iron. These species account for a total 2.5% in the case of the powder derived from the spherical oxide and a total close to 2.1% for the other ones, which contain less oxygen.

Thus, the use of metastable chromium oxides as starting compounds is beneficial for the preparation of Cr_3C_2; indeed, it allows to work at a lower temperature and for a shorter time than has previously been reported (20-22). In a future paper, we will show how with minor modifications of the present carburization conditions metastable chromium carbide Cr_3C_{2-x} (9, 10, 21) can be obtained either alone or mixed with Cr_3C_2. SEM micrographs of the different oxides and carbides are shown in Fig. 2.

Both the oxides and carbides have the same morphology as the oxalates from which they are derived. One can identify needles, rods, spheres and polyhedra. The grains are homogeneous in size and present a very low degree of agglomeration. There is not much difference in average grain size between the oxides and carbides for the needle-shaped (70 x 10 μm), rod-shaped (70 x 20 μm) and polyhedral (30 μm) specimens, whereas the size of the spheres deduced from measurements on SEM micrographs decreases from 9 μm in the oxide to 7 μm in the carbide (Fig. 3). As shown by Lerch and Rousset (23), the so-called "spheres" are in fact made up of aggregates of small platelets. This is evidenced by a higher magnification SEM micrograph (Fig. 4a) showing the "gypsum flower" texture of the oxide. The platelets are approximately 1.5 μm wide and 0.7 μm thick. Upon carburization, these platelets sinter and give the appearance of a crumpled sphere made up of primary crystallites approximately 0.1 μm in size (Fig. 4b).

The specific surface area (S_w) of the different oxides and carbides are reported in Table 2. The S_w of the oxides considerably varied with the morphology, from 280 m^2/g for the needles to 185 m^2/g for the polyhedra and the loss in S_w after carburization varies accordingly (Table 2). As a result, the spherical carbide has a slightly higher S_w (10.9 m^2/g) than the needles and rods (10.0 m^2/g) and than the polyhedra (9.1 m^2/g). Albeit the difference between these values is not high, they clearly account for the less monolithic texture of the spheres compared to the other specimens, as shown by the SEM observations.

Oxidation of the Carbides. The TGA and DTG curves obtained for the different carbides are shown in Fig. 5. Considering the presence of free C and other species in the carbides (see above), the weight gain (Table 3)corresponds in all cases to a total conversion of Cr_3C_2 into Cr_2O_3 (the theoretical weight gain is 26.67%. XRD patterns analysis indeed confirmed that the final product is only constituted of Cr_2O_3, and SEM observation revealed that no change in morphology and size

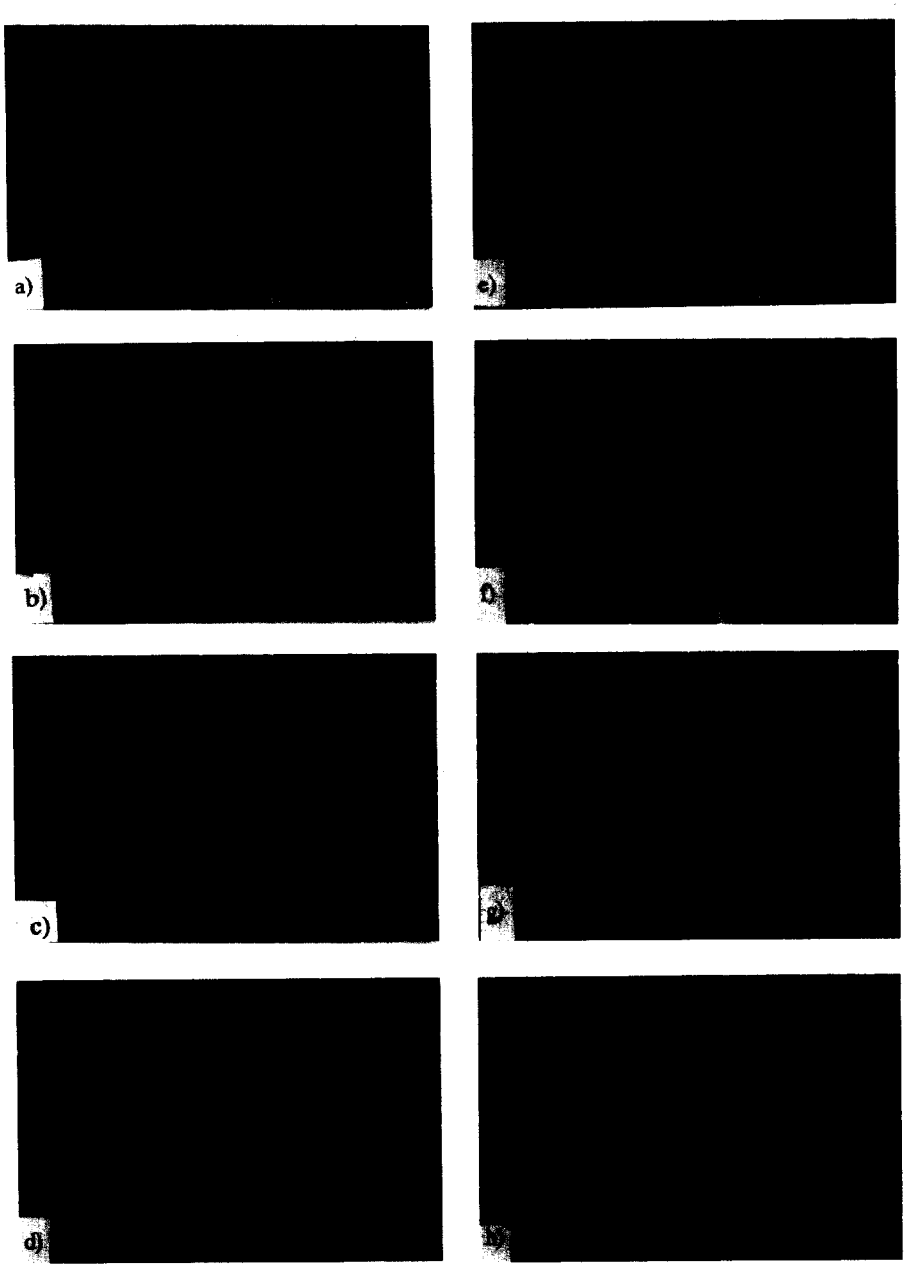

FIG. 2

SEM micrographs of the different chromium oxides: (a) needles; (b) rods; (c) spheres; (d) polyhedra, and (e, f, g, h, respectively) the corresponding carbides.

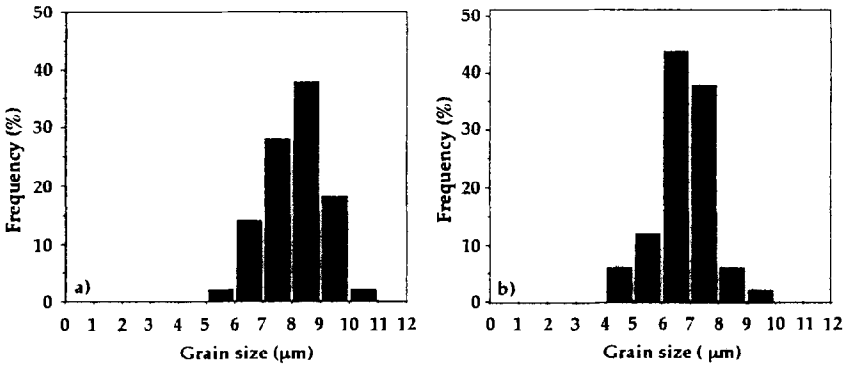

FIG. 3

Grain size distribution of the spherical oxide (a) and carbide (b) deduced from measurements on SEM micrographs.

had occurred (Fig. 6). The four TGA curves have the same shape. Obviously, as evidenced by the DTG curves, the oxidation takes place in several steps. The temperatures at beginning and end of the oxidation, as well as the difference between them, and the temperatures corresponding to the different oxidation peaks (T_1, T_2, T_3, and T_4) are reported in Table 3.

The oxidation begins at a temperature (T_b) close to 300°C (except for the polyhedra, 205°C), but ends at a temperature (T_e) which varies with the morphology. Thus, it is the lowest (618°C) for the spherical grains which have the most rapid reoxidation kinetics, as shown by the difference between T_e and T_b. At the opposite, the polyhedral carbide has the highest T_e (673°C) and the lowest T_b and, therefore, the slowest reoxidation kinetics. The needle-shaped and rod-shaped carbides have similar oxidation behaviour, which is intermediate between the former ones. One can note that these results are in good agreement with the S_w and texture of the different carbides. TheDTG curves (Fig. 5 and Table 3) show that the higher weight gain occurs during the third step except for the polyhedral specimen in which the fourth phenomenon is the prominent one. It seems that the evolution of T_i (i = 1, 2, 3, 4) with the morphology is similar to that of T_e (viz. lower values for the spheres, intermediate values for the needles and rods and higher values for the polyhedra).

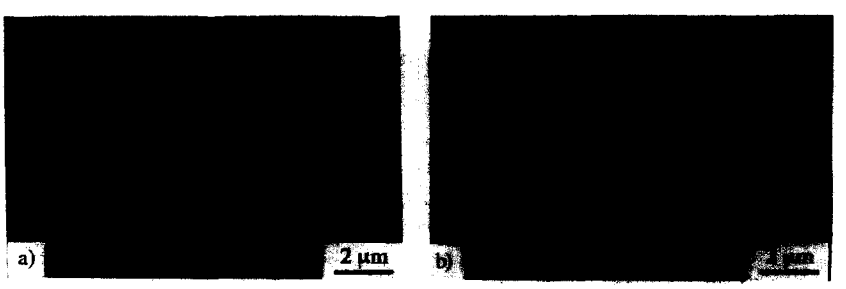

FIG. 4

Higher magnification SEM micrographs of the spherical oxide (a) and carbide (b).

TABLE 2

Specific Surface Area (S_w) of the Different Oxides and Carbides

Morphology	Needles	Rods	Spheres	Polyhedra
S_w oxide (m^2/g)	280	260	240	185
S_w carbide (m^2/g)	10.0	10.0	10.9	9.1
S_w loss (%)	96.4	96.2	95.5	95.1

In order to get more precision, the oxidation of the carbide powders was studied using a DSC calorimeter. The DSC curves (Fig. 7) confirm that the oxidation proceeds in four stages characterized by four exothermal effects in the 300-600°C range (Table IV). The first three peaks occur at nearly the same temperature (approximately 358°, 423°, and 515°C, respectively) regardless of the morphology. On the contrary, it seems that the temperature of the fourth peak varies with the morphology. It is the lowest (555°C) for the spherical carbide and the highest (577°C) for the polyhedral one.

The activation energy (E) corresponding to each stage of the reoxidation process was calculated using Kissinger's theory (25). Analyses were carried out in nonisothermal mode, using displacement of the different peaks as a function of the heating rate. The different activation energies (Table 4) were then deduced from the slope of the linear function $\text{Ln}(a/Tm^2) = f(1/Tm)$ where a is the heating rate and Tm is the temperature corresponding to the top of the peak. One can see that E regularly increases from the first peak (about 110 kJ/mol) to the fourth one (about 200

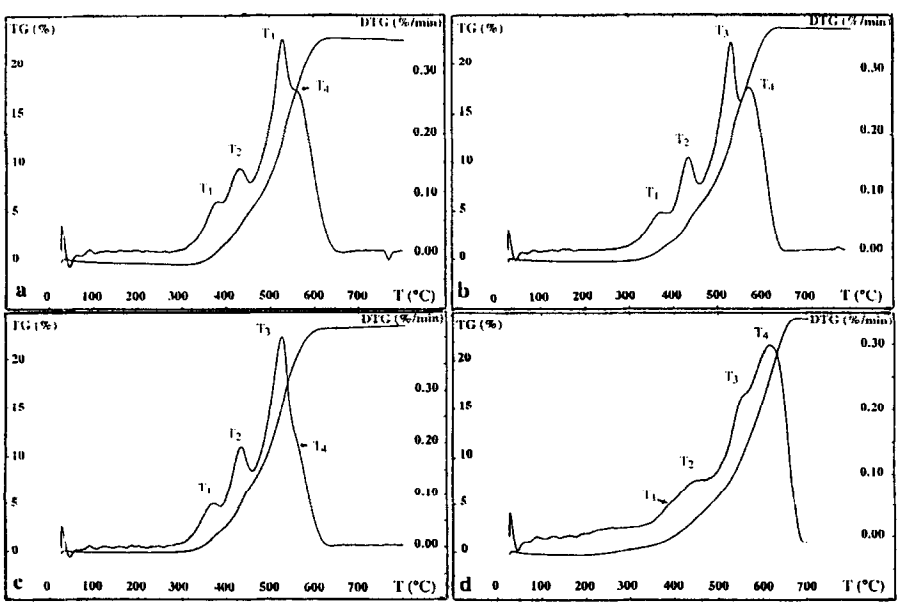

FIG. 5

TGA and DTG curves of the different carbides oxidized in air: (a) needles; (b) rods; (c) spheres; (d) polyhedra.

TABLE 3

Weight Gain and Phenomena Temperatures as Deduced from TGA and DTG

Temperature (°C)	Needles	Rods	Spheres	Polyhedra
T_b	282	282	270	205
T_1	380 (7.7)	373 (6.9)	371 (9.8)	380 (1.9)[a]
T_2	432 (16.6)	434 (17.2)	433 (21.4)	452 (17.1)
T_3	531 (48.5)	532 (42.8)	525 (50.2)	557 (27.6)
T_4	566 (27.2)	574 (33.1)	561 (19.2)	618 (53.4)
Te	640	640	618	673
T_e-T_b	358	358	348	468
Weight gain (%)	23.09	23.93	23.51	24.57

T_b: temperature of oxidation beginning; T_i (i = 1, 2, 3, 4): temperature of the i^{th} peak;T_e: temperature of oxidation end. Number in parentheses is the proportion to the total weight gain.
[a]This peak is partially masked by peak 2; the weight gain corresponds to the oxidation between T_b and T_1.

kJ/mol). The latter one only varies significantly with the carbide morphology, in the same way as the corresponding temperature.

It has been shown (26, 27) that when Cr_3C_2 is exposed to air or oxygen, carbon is predominantly oxidized and there is formation of the lower Cr_7C_3, $Cr_{23}C_6$ carbides and probably also of metallic chromium at the interface between the oxide layer and the remaining carbide. Paris and Clar (20) mention that a fine-grained Cr_3C_2 powder is totally oxidized between 370°C and 700°C but do not detail the oxidation process. Korablev et al. (28) have performed oxidation tests on a commercial Cr_3C_2 powder and have reported an oxidation in three steps in the 800-1100°C range. They have represented the oxidation process of chromium carbide in the following manner:

$$Cr_3C_2 \rightarrow Cr_7C_3 \rightarrow Cr_{23}C_6 \rightarrow [Cr] \rightarrow Cr_2O_3$$

Korablev et al. (28) connected the exothermal effects with the formation of Cr_7C_3, $Cr_{23}C_6$ and Cr for the first, second, and third peaks, respectively, the last one also corresponding to a complete oxidation of the bulk product. A careful examination of their data (28) reveals a shoulder on the high temperature side of the third peak, corresponding to the fourth phenomenon observed in the present study. Their conclusions were supported by XRD patterns analysis of the powders quenched after each oxidation peak, which revealed the presence of Cr_7C_3 and $Cr_{23}C_6$. In our case, the XRD patterns of the products quenched after each peak (Fig. 8) only showed the presence of both Cr_3C_2 and Cr_2O_3, the amount of the latter increasing with the increase in temperature. We suggest that the Cr_7C_3, $Cr_{23}C_6$ and Cr species formed upon oxidation in our powders are thermodynamically unstable under the experimental conditions and therefore become oxidized straight away. A very small amount could be present at the interface between the oxide layer and the unreacted Cr_3C_2, but TEM observation of a quenched product do not reveal the presence of

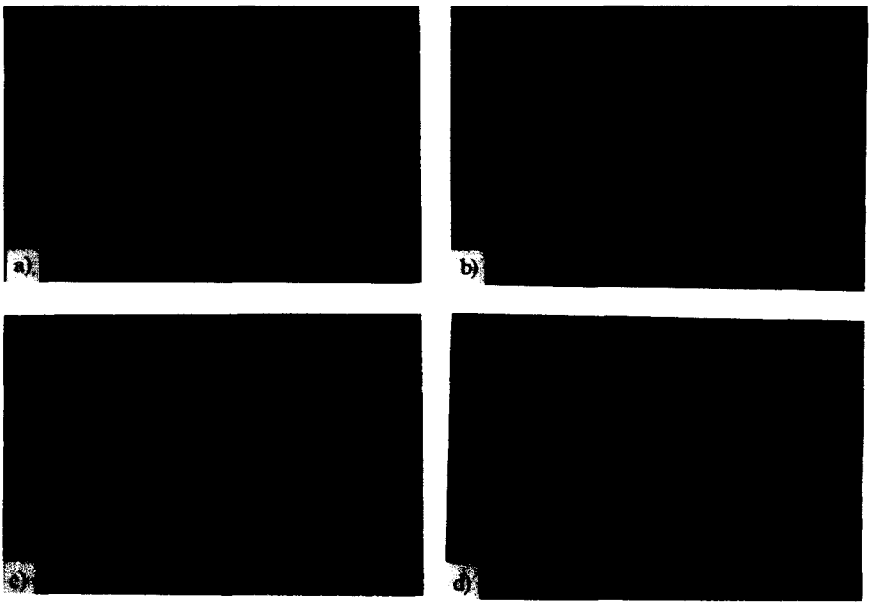

FIG. 6
SEM micrographs of the oxides obtained after oxidation of the different carbides: (a) needles; (b) rods; (c) spheres; (d) polyhedra.

such an interphase (Fig. 9) and only Cr_3C_2 and Cr_2O_3 were detected by electron microdiffraction patterns analysis. Other researchers (29, 30) have also reported that in the case of an incomplete oxidation of Cr_3C_2, the remaining carbide material could be the same as the starting one.

Comparing the oxidation behaviour of the needle-shaped, rod-shaped, spherical and polyhedral carbides, the above thermal analysis data show that the main difference is a shift in the fourth peak temperature and activation energy. According to Korablev et al. (28), one can consider that several phenomena contribute to an oxidation step: the formation of a given compound, its oxidation into Cr_2O_3 and the diffusion of oxygen through the precedently formed oxide layer. The latter one is to be taken more and more into account as the reaction proceeds and depends on the morphology and texture of the powder. Since the grains of the spherical carbide are made up of small crystallites, at the difference of the other specimens which are more monolithical, oxygen diffusion towards the interior of this material is easier owing to a much shorter diffusion path. The polyhedral grains are the more monolithical and thus the temperature, proportion and activation energy of the fourth peak are the higher.

CONCLUSIONS

Cr_3C_2 powders have been elaborated by heat-treatment of metastable chromium oxides of controlled morphology in H_2-CH_4 atmosphere. Owing to the high reactivity of these starting oxides, 700 °C is a sufficiently high carburization temperature to obtain Cr_3C_2 only. The reaction is pseudomorphic and different grain shapes (needles, rods, spheres and polyhedra) have been

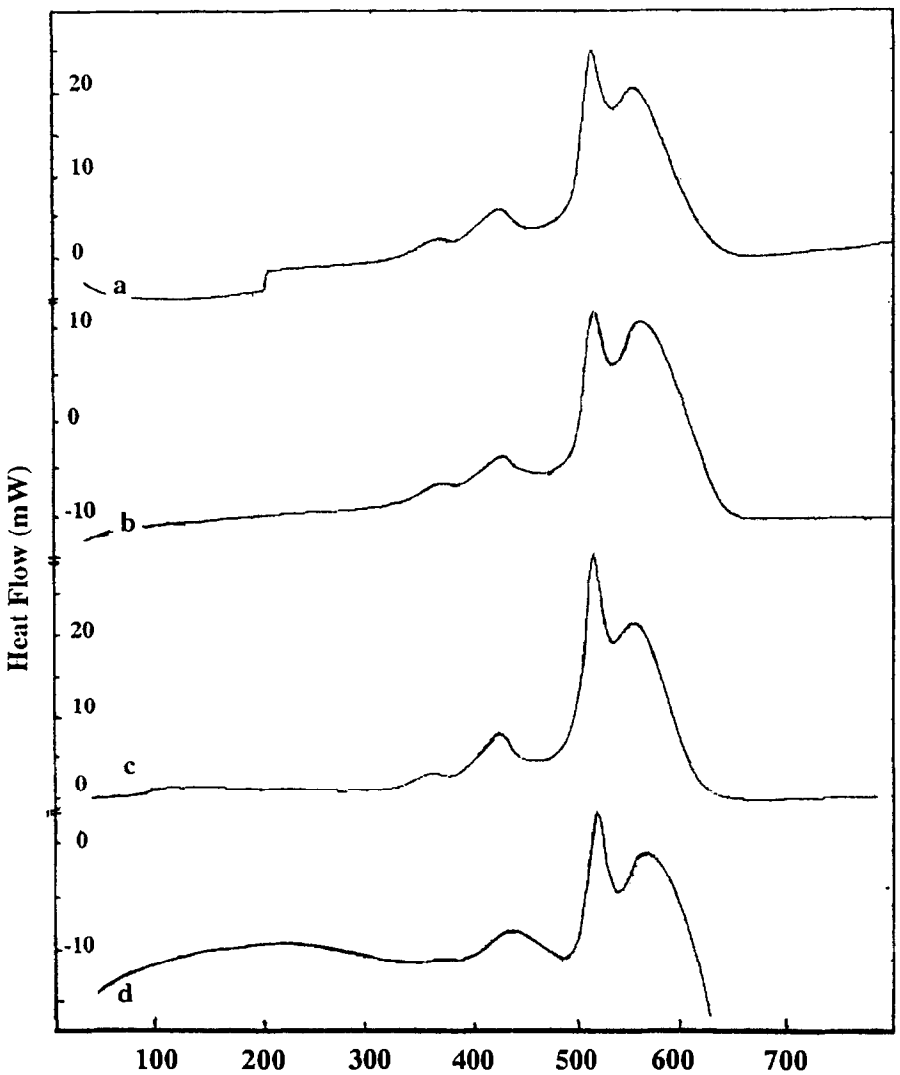

FIG. 7

DSC curves of the carbides oxidized in air: (a) needles; (b) rods; (c) spheres; (d) polyhedra.

obtained. The size distribution is narrow and the grain size is of the order of a few tens of micrometers, but the spheres are in fact made up of aggregates of small platelets approximately 1.5 μm wide and 0.7 μm thick and have a "gypsum flower" texture. The oxidation in air of the carbides proceeds in four steps in the 250-700°C range, which is much lower than for commercial specimens. The first three steps are related to the formation and the quasi-immediate oxidation of Cr_7C_3, $Cr_{23}C_6$, and probably Cr, while the last one corresponds to the oxidation of the remaining material due to a complete diffusion of oxygen through the already formed oxide layer. Differences in oxidation behaviour between the carbides mostly are in the temperature and activation energy

TABLE 4
Temperature (T in °C) and Activation Energy (E in kJ/mol) of the Exothermal Peaks (DSC)

	Needles		Rods		Spheres		Polyhedra	
Peak n°	T	E	T	E	T	E	T	E
1	358	114	358	114	357	110	358	114
2	423	135	423	135	419	130	424	135
3	515	165	515	165	514	160	515	165
4	565	209	565	209	555	170	577	216

of this last phenomenon. Both are significantly lower for the spherical carbide, which is less monolithical ("gypsum flower" texture) than the other specimens. Intermediate values are observed for the needles and rods, and the higher values for the polyhedral grains.

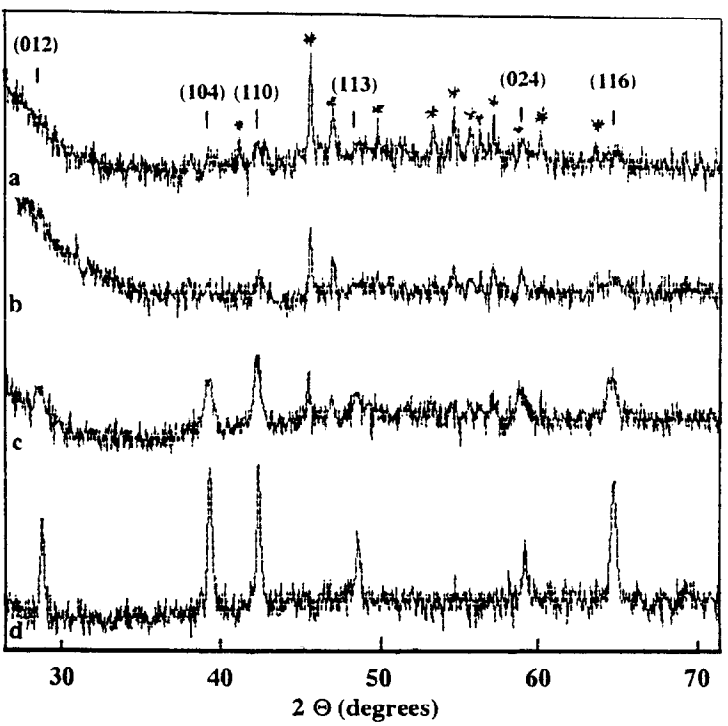

FIG. 8
XRD patters of the oxidation products after quenching at temperature T_1 (a), T_2 (b), T_3 (c), and T_4 (d) (spherical specimen). *: Cr_3C_2; indexed: Cr_2O_3.

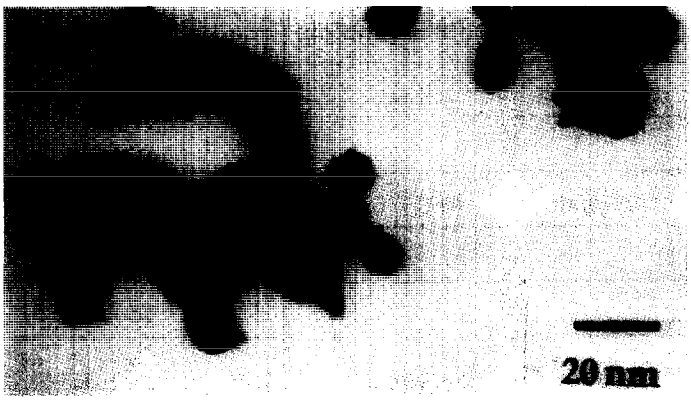

FIG. 9
TEM micrograph of the spherical specimen quenched at 495°C.

REFERENCES

1. L.E. Toth, Transition Metal Carbides and Nitrides, Academic Press, New York (1971).
2. S.C. Chuang, C.T. Kuo, C. S. Lee, C. T. Ho, and A.K. Li, J. Mat. Sci. **27**, 5844 (1992).
3. C.T. Ho, J. Mater. Res. **8**, 2035 (1993).
4. S. Komiya, S. Ono, N. Umezu and T. Narusawa, Thin Solid Films **45**, 433 (1977).
5. G. Cholvy, J.L. Derep, and M. Gantois, Thin Solid Films **126**, 51 (1985).
6. K. Bewilogua, H.J. Heinitz, B. Rau, and S. Schulze, Thin Solid Films **167**, 233 (1988).
7. K. Bewilogua, E. Bugiel, B. Rau, C. Schürer, and C. Weissmantel, Krist. Tech. **15**, 1205 (1980).
8. M. Naka, S. Hanada, and I. Okamoto, in Rapidly Quenched Metals (S. Steeb and H. Warlimont, Eds.), p. 361, Elsevier Science Publishers B.V., Amsterdam (1985).
9. E. Bouzy, G. Le Caër, and E. Bauer-Grosse, Philos. Mag. Letters **64**, 1 (1991).
10. E. Bouzy, E. Bauer-Grosse, and G. Le Caër, Philos. Mag. B **68**, 619 (1993).
11. F. Maury, Appl. Organomet. Chem. **6**, 619 (1992).
12. G. Le Caër, E. Bauer-Grosse, A. Pianelli, E. Bouzy, and P. Matteazzi, J. Mat. Sci. **25**, 4726 (1990).
13. J. Subrahmanyam and S. Subba Rao, Metals Materials and Processes **4**, 287 (1993).
14. P. Schwarzkopf and R. Kieffer, Refractory Hard Metals, Macmillan, New York (1953).
15. T. Kosolapova and G. Samsonov, Zhur. Prikl. Khim. **32**, 1505 (1959).
16. V.V. Grigorieva and V N. Klimenko, Akad. Nauk SSSR Inst. Met. **4**, 317 (1959).
17. W.F. Chu and A. Rahmel, Oxidation of Metals **15**, 331 (1981).
18. A.A. Popov, P.H. Ostrik and H.H. Gasik, Tzv. Vuz. Chernaya Metall. **10**, 1 (1986).
19. Philips Gloeilampen Fabrieken N.V., Dutch Patent n° 89-609 (1954).
20. R.A. Paris and E. Clar, Chimie et Industrie-Génie Chimique **99**, 255 (1968).
21. D. Thibaudon, M. Roubin, R.A. Paris, and J. Paris, Planseeber. Pulvermetal. **20**, 129 (1972).
22. R. Bugarel and H. Gros, Chimie et Industrie-Génie Chimique **105**, 1265 (1972).
23. A. Lerch and A. Rousset, Thermochim. Acta **232**, 233 (1994).
24. D.D. Wagman, J.E. Kilpatrick, W.J. Taylor, K.S. Pitzer and F.D. Rossini, J. Res. Nat. Bur. Stand. **34**, 143 (1945).
25. H.E. Kissinger, J. Res. Nat. Bur. Stand. **57**, 217 (1956).
26. V.A. Lavrensko and A.P. Ponytkin, Dokl. Akad. Nauk. SSSR **221**, 130 (1975).
27. R.F. Voitovich, "Oxidation of carbides and nitrides," Naukova Dumka, Kiev (1981).
28. S.F. Korablev, A.V. Lysenko and S.I. Filipchenko, Soviet Powder Metallurgy and Metal Ceramics **27**, 584 (1988).
29. W.M. Dawson and F.R. Sale, Metall. Trans. A **8A**, 15 (1977).
30. C.T. Fu, A.K. Li, and J.M. Wu, J. Mat. Sci. **28**, 6285 (1993).